J Mater Sci (2010) 45:759–764
DOI 10.1007/s10853-009-3997-3

Strain localization of fully dense nanocrystalline Ni sheet

Rongtao Zhu · Jianqiu Zhou · Hua Jiang · Dongsheng Zhang

Received: 1 September 2009 / Accepted: 28 October 2009 / Published online: 12 November 2009

Abstract The fully dense electrodeposited nanocrystalline Ni sample with dimensions at tens of millimeters was characterized under quasi-static uniaxial tensile load. During testing, the sample exhibited high strength simultaneously with a decrease in tensile strain. To inspect this early failure of the nanocrystalline Ni sample in this article, the strain fields of the sample were quantified with digital image correlation algorithm, and strain localization phenomenon in the form of shear band was captured successfully. Meanwhile, the failure mode and fracture surface of the Ni sample were examined in detail. The results suggest that the shear banding is a main deformation mode in nanocrystalline Ni sample, and it is an important factor to induce the early failure of the sample during plastic deformation.

Introduction

Nanocrystalline (NC) metals have been a source of great interest currently due to their unusual mechanical properties, such as high yield and fracture strengths [1–3], better wear resistance [4, 5], improved magnetic properties [6], and superplasticity at some special cases [7, 8]. However, it should be noted that the strength increases simultaneously with a decrease in tensile strain due to high propensity of NC materials to deformation localization [9], and it has been a major obstacle in the development and application of the materials. While the limited ductility was previously attributed to be pre-existing flaws, such as impurities and porosity [10], recent examples of good quality still show a little ductility in tension [11–13]. Thus, the ductility issue remains an important subject of present research. Several scientists [12–22] have associated the limited ductility with plastic flow localization in the form of shear band in a wide range of deformation operations based on their novel experimental and numerical investigations. From their results, shear localization is an important deformation mode in NC metals, and it will develop with strain and contribute to the early failure during plastic deformation. Meanwhile, it is affected by many factors, such as grain size and its distribution, strain rate, temperature, and grain boundary angle. However, quantitative experimental studies for explaining and describing the critical condition for shear localization nucleation and propagation have not previously been reported. Motivated by this consideration, a quantitative experimental study on the shear localization of NC Ni sheet subjected to quasi-static uniaxial tensile load was carried out in this article. Commercially available NC electrodeposited Ni was chosen for the reason that its mechanical properties reported in the literatures vary over a very small range [23, 24] and the electrodeposition method is capable of producing relatively larger dimension of a full-dense metal for conventional tensile test in a single batch. Meanwhile, digital image correlation (DIC) technique, which is an in situ, noncontacted, non-destructive correlation method, was used to measure surface strain fields of the NC Ni during deformation

R. Zhu · J. Zhou (✉) · H. Jiang
School of Mechanical and Power Engineering, Nanjing University of Technology, Nanjing, Jiangsu 210009, China
e-mail: zhouj@njut.edu.cn

D. Zhang
Department of Mechanics, Shanghai University, Shanghai 200444, China

D. Zhang
Shanghai Institute of Applied Mathematics and Mechanics, Shanghai 200072, China

process. Evolution of strain localization in the NC Ni sample was imaged through the DIC algorithm at different strain value, and the strain localization zones were examined through field emission scanning electron microscope (FESEM). Finally, the failure mode and fracture surface of the sample were investigated in detail. The results show that the strain localization in the form of shear banding is a main factor resulting in the early failure of the NC Ni sample.

Experimental

Larger dimension (76.2 mm × 76.2 mm × 0.2 mm thick) commercially available NC electrodeposited fully dense Ni sheets with a purity of 99.9% were purchased from Integran Technologies Inc. (Canada). Their nominal grain sizes are about 20 nm. The sheets had an initial thickness of about 200 μm and were polished on one side using SiC paper with diamond suspensions of 3, 1, and 0.25 μm grain sizes, respectively. After the polishing procedure, the thickness of the sheets reached 150 μm.

First, dog-bone-shaped tensile samples were electrodischarge machined from the polished NC sheets for DIC studies. The width and length of the tensile sample gage section are 10 and 30 mm, respectively, while thickness is approximately 150 μm. These tensile samples have centimeters in gage section that allow conventional tensile tests.

Second, the tensile sample was loaded at room temperature with Zwick BZ2.5/TS1S universal test machine at a quasi-static strain rate of 10^{-4} s^{-1}. To minimize out-of-plane loading and displacement, two grips of the test machine were carefully aligned. Moreover, the knurl grips were used to minimize slippage between grips and sample. Meanwhile, at the normal of the sample, a video camera (Model JAI CV-A1) was used to acquire images of the sample surface during loading and linked to computer to record the images. Sequential images were acquired at a constant frequency of 0.5 Hz during loading. Data acquisition stopped when the sample was fractured.

Finally, DIC algorithm was used as an optical strain gage to measure strain developed on the sample surface with the increase of loading. This method has been applied to deal with the mechanics of materials [25–27] due to the relative simplicity and low cost. Each subset represented a square region approximately 210 μm × 210 μm. The step size that defined the number of pixels over which the subset is shifted in longitudinal and transverse directions to calculate the next result was 1 pixel. Moreover, the strain localization zones and the fracture surface of the tested NC sample were examined with a JEOL 6400 FESEM operated at 20 kV.

Results and discussion

Figure 1 shows engineering stress–strain curve of the NC Ni obtained during quasi-static tensile loading at a strain rate of 10^{-4} s^{-1}. It is clear that the NC Ni exhibits a relatively higher strength, but the ductility is limited compared with the coarse-grained counterpart. Moreover, lack of strain hardening behavior after an initial stage of strain hardening over a small plastic strain regime is exhibited for the NC sample. Similar results were reported by several other groups for NC metals [28–30]. The small or negative strain hardening behavior can be attributed to the fact that the extremely small grains in NC metals cannot store dislocations to increase defect density by orders of magnitude as normally possible in coarse-grained metals and thus the nonhomogeneous plastic deformation occurs in NC metals. Obviously, the engineering stress–strain curve of the NC Ni in this experiment can be divided into three stages. As shown in Fig. 1, stage I corresponds to elastic deformation (before yield point), and stage II, corresponding to strain hardening regions, holds about 2% plastic strain (after yield point). In stage III, the apparent negative slope in the tensile engineering stress–strain curve can be observed. This may suggest the appearance of nonhomogeneous plastic deformation in the NC Ni sample.

To monitor the plastic deformation process of the NC Ni sample, the in situ DIC method that based on direct, observational, quantitative evidence was used and some critical points, such as shear localization nucleation, broadening process, and failure point were recognized. Figure 2 shows strain maps of the sample in longitudinal and transverse directions calculated by the DIC algorithm, which correspond to consecutive points taken at different strain values indicated by the data signs (a, b, c, d, e, and f) on the stress–strain curve in the Fig. 1. Apparently, strain

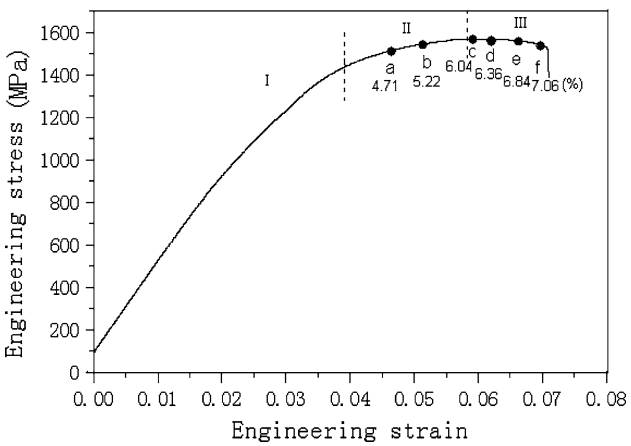

Fig. 1 Engineering stress–strain curve of the fully dense electrodeposited NC Ni. The data signs (*a*, *b*, *c*, *d*, *e*, and *f*) present the strain values; the numbers beneath the data points are the strain value

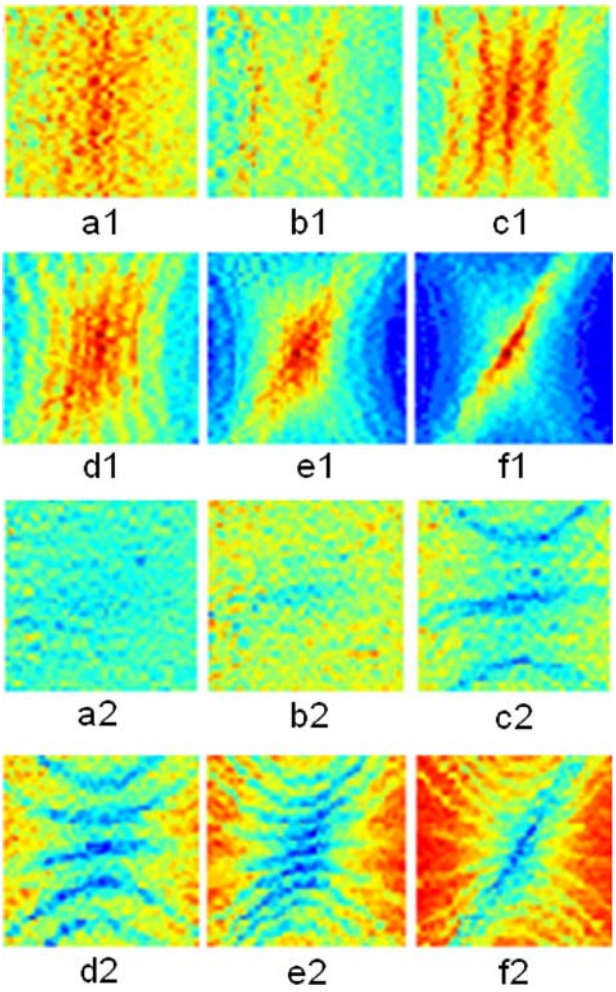

Fig. 2 Strain maps of the NC Ni sample in longitudinal (**a1**, **b1**, **c1**, **d1**, **e1**, and **f1**) and transverse (**a2**, **b2**, **c2**, **d2**, **e2**, and **f2**) directions calculated by DIC algorithm corresponding to consecutive points taken at different strain values indicated by the data signs (*a*, *b*, *c*, *d*, *e*, and *f*) on the stress–strain curve in Fig. 1

distribution is uniform at initial range after the yield point (point a). When the strain reaches the value of 5.22%, the evidence of strain localization begins to occur (point b). Although the onset of strain localization was observed in the strain hardening stage (stage II), its development is very slow in this stage. In contrast, rapid evolution of the strain localization is exhibited in the strain softening stage (stage III). In longitudinal direction, at early stage of strain softening, deformation of the sample becomes more concentrated on several local regions (c1). With increasing strain, the strain localization zones shown in the following strain map (d1) become dense, and the existing zones begin to bend into middle area of the sample. These zones on the two sides of the middle line of the sample form a symmetric pattern. The following map (e1) corresponds to the further softening in stress–strain curve. In this map, new strain localization zones do not develop continually, but the existed strain localization zone have become more inclined and have seemingly evolved to two conjugate direction banded structures across the overall surface of the sample. The last strain map (f1) precedes failure point of the sample, at which one of the two conjugate strain localization zones is clearly dominant compared to the previous maps. At the same time, in transverse direction, strains appear to be concentrated within back-to-back "V" pattern zones at early stage of softening (c2). Similar to the strain maps in longitudinal direction, the following maps (d2) show that the strain-concentrated zones of the "V" patterns developed gradually from upper and lower boundary of the sample to the center of the field, respectively, which also leads to the intensification of the strain localization zones on the middle side of the sample. Eventually, the connection of the upper and lower concentrated zones forms two conjugate shear localization zones that also can crossover completely the sample (e2). In the last map (f2), one shear localization zone is clearly dominant too, which have a good agreement in inclination with the fully formed strain localization zones in longitudinal direction.

Comprehensive investigations of the evolution of strain localization in longitudinal and transverse indicate that the pattern of multiple, conjugate-banded structures is produced in the NC Ni sample under uniaxial tensile loading. The evolution process of plastic deformation in the Ni sample reveals that the strain localization can propagate with two different patterns: a number of parallel shear bands with oppositely direction and many shear bands oriented along the conjugate direction. In the early stage of softening region, the strain localization only appear in local area, thus there is no clear path for shear band to evolve and the sample cannot fail immediately. However, when the conjugate strain localization zones form across the overall surface of the sample, a competition between opposing directional tendencies of the conjugate-oriented strain localizations occurs during the plastic deformation process of the Ni sample. It is only after one of the strain-banded structure wins the competition or single strain localization zone is dominant in plastic deformation, the fracture of the sample will be observed.

More detailed structures of the strain localization zones were revealed by FESEM to determine the fracture mechanism of the sample, which was shown in Fig. 3. In this figure, a series of parallel shear lines which can also be called bundle of shear band were shown. The majority of individual shear band lines have a width in sub-micrometer range (0.3–0.8 μm). Wei et al. [15] have also observed experimentally dense network of multiple shear bands in nanostructure Fe under quasi-static compression test. Meanwhile, the inclination of shear band lines is very close to that of strain localization zones mentioned above. So we

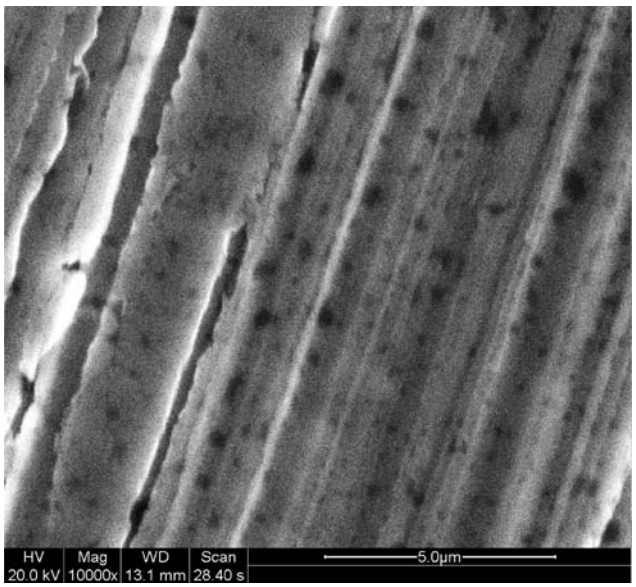

Fig. 3 FESEM micrograph of the strain localization zones of NC Ni under quasi-static tensile loading

can treat the localized deformation zones as an assemblage of dense shear band lines.

In this article, abundant data calculated from the DIC algorithm can be used to infer the failure model of NC Ni sample based on distribution of maximum in-plane shear strain, γ_{max}, for the full formation shear localization zone. The maximum in-plane shear strain γ_{max} can be expressed as

$$\gamma_{max} = \left[\left(\varepsilon_x - \varepsilon_y \right)^2 + 4\gamma_{xy}^2 \right]^{1/2}. \quad (1)$$

Figure 4a shows the distribution curves of maximum in-plane shear strain for the point f in Fig. 1 at different position along transverse direction. It is clear that the primary peak of maximum in-plane shear strain shifted to the center step by step, and the shear strain reached maximum at the center of the sample. This indicates that the sample will fail first in the middle of the sample and shear strain is dominant in full formation shear localization zones. This behavior can be verified by more solid evidences. Figure 4b shows the image captured prior to the fracture of the sample. From this figure, crack initiates in the center of the sample, which have a good agreement with the experimental results calculated by the DIC method. Figure 5 shows the fracture pattern of the NC Ni sample. It is clear that the angle of the failure plane of the NC sample with respect to the loading axis was very close to 63°. The inclination of failure plane is very close to that of strain localization zones monitored by DIC method and the shear band bundle observed by FESEM. This indicates that shear banding is the main deformation mode in NC Ni sample.

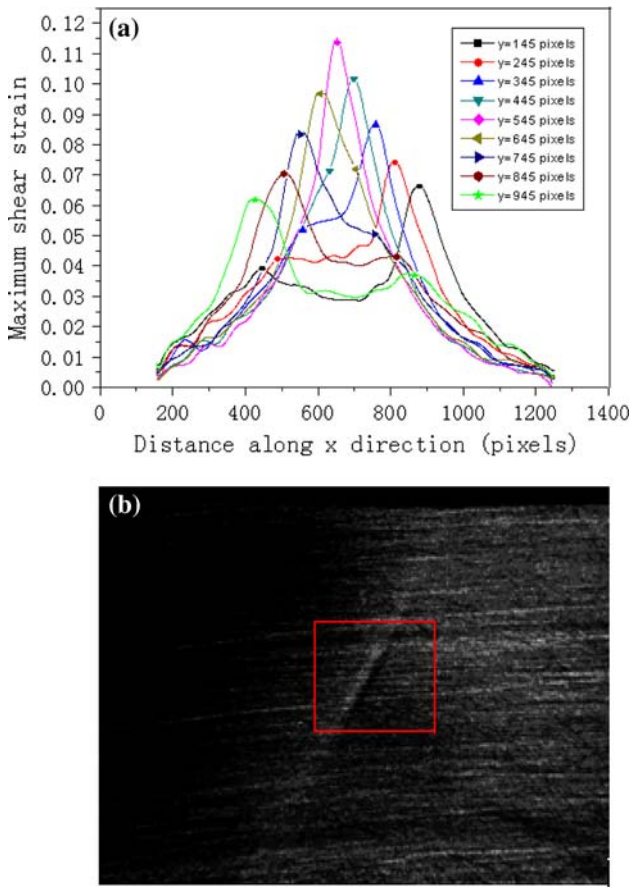

Fig. 4 **a** Distribution of in-plane maximum shear strain at different position along transverse direction. **b** The image prior to the fracture of the sample, the crack initiates in the middle of the sample

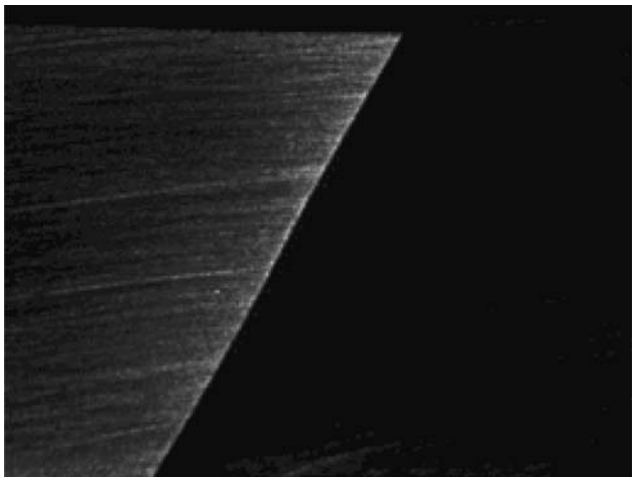

Fig. 5 Fracture pattern of the fully dense NC Ni

To inspect the failure mechanism of the NC Ni sample further, the facture surface was examined by FESEM too. Figure 6 shows the FESEM micrographs of details of the fracture surface after tensile test. A low-magnification

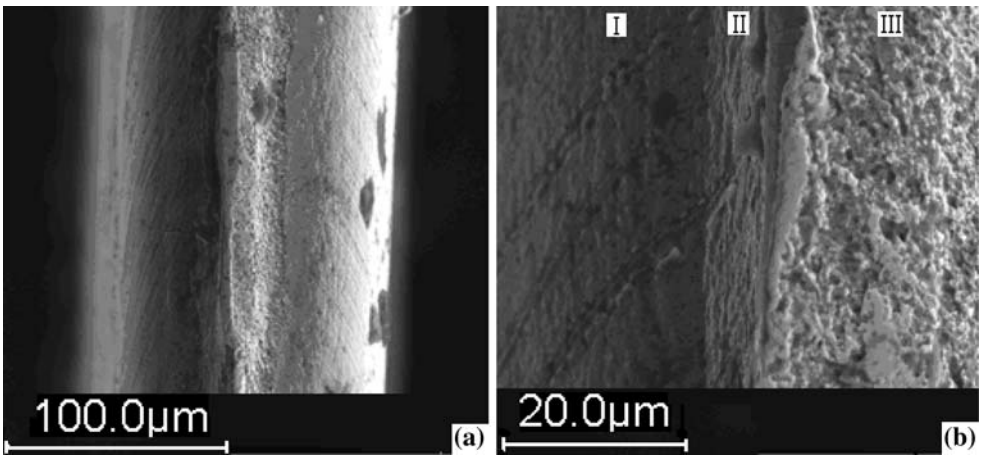

Fig. 6 SEM micrographs of fracture surface of the NC Ni sample. **a** Low-magnification image shows a symmetry pattern of fracture structure. **b** Enlarged image of left side of **a** exhibits three different fracture structures

SEM micrograph (Fig. 6a) exhibits a symmetry pattern of fracture structure. Furthermore, enlarged image of the micrograph shown in Fig. 6b exhibits a "sandwich" structure. Within the fracture surface, three different structures, marked by the symbols I, II, and III, could be clearly observed. Sliding planes, in which several sliding bands can be observed, appear at left edge of this image, while ductile facture with dimpled features was observed in right edge of the image. Meanwhile, apparent striations were found in the middle of the fracture surface. This fracture morphology suggests that a mixture of micro-mechanism play a role in the deformation of NC sample. First, the dislocation pile-up mechanism is dominant in strain hardening stage [31], which exhibits ductile fraction as characterized by the dimple feature. Then, the shear banding mechanism initiates. With the development of the strain softening behavior, this mechanism become dominant gradually and the dislocation mechanism may cease. Eventually, the region II of fracture surface suggests that the tensile sample may have been torn apart in a rather brittle manner because the sample cannot sustain the more plastic strain when the full formation shear localization generates.

Conclusions

The electrodeposited fully dense NC Ni sample has high strength but poor ductility during the tensile test. The limit ductility is attributed to the strain localization in form of shear band lines. To monitor the plastic deformation process of the NC Ni sheet subjected to quasi-static uniaxial tensile load, the DIC method was used in this article. Evolution of surface strains in the sample was imaged by the DIC algorithm and some critical points, such as shear localization nucleation, developing process and failure point were recognized. First, the onset of shear localization was observed at the tail range of strain hardening stage after the uniform deformation in initial range. At the strain softening stage, the propagation of the shear localization is very rapid and multiple, conjugate banded structures was produced in the NC Ni sample. Finally, when the prime full-developed banded structure wins the competition between opposing directional tendencies of the conjugate-oriented strain localization zones, the fracture of the sample can be observed. Moreover, the detailed structures of the strain localization zone were examined. The result shows that the strain localization zone is an assemblage of dense shear band lines. Meanwhile, the failure mode and the fracture surface were investigated to verify the fracture mechanism in the NC Ni sample. The results indicate that crack initiates first in the middle of the sample, and the shear banding is an important factor to induce the failure of the sample.

Acknowledgements This work was supported by National Natural Science Foundation of China (10502025, 10872087), Natural Science Foundation of Jiangsu Province (BK2007528), University Graduate Innovation Plan of Jiangsu Province (CX09B_129Z), and Doctors' Innovation Foundation of NJUT (BSCX200814).

References

1. Suryanarayana C (1995) Int Mater Rev 40:41
2. Masumura RA, Hazzledine PM, Pande CS (1998) Acta Mater 46:4527
3. Wang YM, Huang JY, Jiao T, Zhu YT, Hamza AV (2007) J Mater Sci 42:1751. doi:10.1007/s10853-006-0822-0
4. Farhat ZN, Ding Y, Northwood DO, Alpas AT (1996) Mater Sci Eng A 206:302
5. Jeong DH, Gonzalez F, Palumbo G, Aust KT, Erb U (2001) Scripta Mater 44:493

6. Vajpai S, Dube R (2009) J Mater Sci 44:129. doi:10.1007/s10853-008-3111-2
7. McFadden SX, Mishra RS, Valiev RZ, Zhilyaev AP, Mukherjee AK (1999) Nature 398:684
8. Lu L, Sui ML, Lu K (2000) Science 287:1463
9. Wang YM, Wang K, Pan D, Lu K, Hemker KJ, Ma E (2003) Scripta Mater 48:1581
10. Weertman JR, Farkas D, Hemker K, Kung H, Mayo M, Van Swygenhoven H (1999) MRS Bull 24:44
11. Schwaiger R, Moser B, Dao M, Chollacoop N, Suresh S (2003) Acta Mater 51:5159
12. Dalla Torre F, Van Swygenhoven H, Victoria M (2002) Acta Mater 50:3957
13. Cheng S, Ma E, Wang YM, Kecskes LJ, Youssef KM, Koch CC, Trociewitz UP, Han K (2005) Acta Mater 53:1521
14. Jia D, Ramesh KT, Ma E (2003) Acta Mater 51:3495
15. Wei Q, Jia D, Ramesh KT (2002) Appl Phys Lett 81:1240
16. Wei Q, Kecskes LJ, Jiao T, Hartwig KT, Ramesh KT, Ma E (2004) Acta Mater 52:1859
17. Carsley JE, Fisher A, Milligan WW, Aifantis EC (1998) Metall Mater Trans A 29:2261
18. Hung PC, Sun PL, Yu CY, Kao PW, Chang CP (2005) Scripta Mater 53:647
19. Sansoz F, Dupont V (2007) Mater Sci Eng C 5–8:1509
20. Fu H, Benson DJ, Meyers MA (2004) Acta Mater 52:4413
21. Wei YJ, Anand L (2004) J Mech Phys Solids 52:2587
22. Warner DH, Sansoz F, Molinari JF (2006) Int J Plast 22:754
23. Mishra AC, Thakur AK, Srinivas V (2009) J Mater Sci 44:3520. doi:10.1007/s10853-009-3475-y
24. Jung A, Natter H, Hempelmann R, Lach E (2009) J Mater Sci 44:2725. doi:10.1007/s10853-009-3330-1
25. Barthelat F, Wu Z, Prorok BC, Espinosa HD (2003) Exp Mech 43:331
26. Florando JN, LeBlanc MM, Lassila DH (2007) Scripta Mater 57:537
27. Canadinc D, Efstathiou C, Sehitoglu H (2008) Scripta Mater 59:1103
28. Koch CC (2003) Nanocryst Mater 18:9
29. Swygenhoven HV, Caro A (1997) Nanostruct Mater 9:669
30. Jia D, Wang YM, Ramesh KT, Ma E, Zhu YT, Valiev RZ (2001) Appl Phys Lett 79:611
31. Li W, Liu P, Ma FC, Rong YH (2009) J Mater Sci 44:2925. doi:10.1007/s10853-009-3386-y